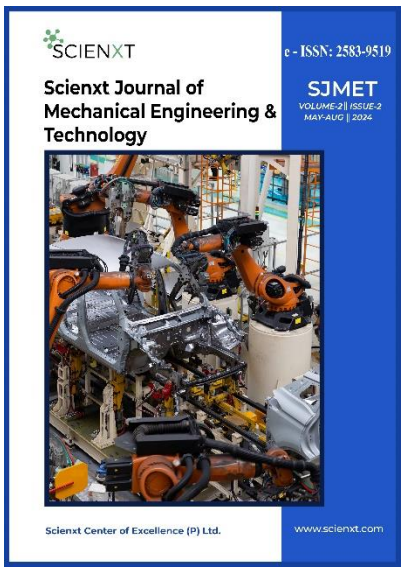

Scienxt Journal of Mechanical Engineering & Technology
Volume-2 || Issue-2 || May-Aug || Year-2024 || pp. 1-18

Using response surface methodology to investigate the effect of TIG welding parameters on the microstructure and corrosion resistance of 2205 DSS welds

[*1]Mohamed S. Melad, [2]Mohamed A. Gebril, [3]Farag M. Shuaeib, [4]Dawod Elabar, [5]Adam H. Alzwi, [6]Mawada S. Elmabrouk

[*1,2,3,4,5,6]Mechanical Engineering Department, Faculty of Engineering, University of Benghazi, Benghazi P.O. Box 1308, Libya

**Corresponding Author: Mohamed S. Melad*
Email: mohamed.melad@uob.edu.ly

Abstract:

Duplex stainless steel DSS offers high corrosion resistance and mechanical strength due to its alloying elements and equal austenite-ferrite ratio. However, in most DSS applications welding is necessary to join part together. Welding DSS affects microstructure and causes precipitation, leading to poor mechanical properties and corrosion resistance. Therefore, this study examines the impact of TIG welding parameters on the microstructure and corrosion resistance of DSS weldments. The corrosion penetration rate CPR of the DSS weldments was determined via electrochemical impedance technique. The correlation between welding variables and corrosion penetration rate was analyzed using response surface methodology and microstructure analysis. Results showed that statistically the welding current and welding speed had the most significant impact on the corrosion penetration rate. Increasing welding current and decreasing welding speed resulted in higher heat input, which led to the formation of Cr_2N precipitation and subsequently, an increase in corrosion penetration rate. On the other hand, low welding current and high welding speed, which correspond to low heat input, increase weld corrosion rates due to higher ferrite content. Adding a small amount of N_2 to Ar as a shielding gas reduces the corrosion penetration rate. However, if the N_2 amount exceeds 10%, it causes the reappearance of Cr_2N precipitates, increasing the corrosion penetration rate. Based on the response surface methodology, the optimum value of TIG welding parameters is welding current 200 a, welding speed 215 mm/min, and 12% N_2 addition with Ar as shielding gas. These TIG welding setups reduce the corrosion penetration rate to 0.0005 mm/y.

Keywords:

Duplex stainless steel, TIG welding process, N_2 shielding gas, Response surface method, corrosion resistance.

1. Introduction:

Duplex stainless steel (DSS) has a unique microstructure consisting of ferrite and austenite, making it superior to other types of stainless steel in terms of its mechanical properties. This combination of microstructure results in increased strength, hardness, and ductility, as well as a higher corrosion resistance than other stainless steels [1]. As a result, DSS has become increasingly popular in many industrial applications, including oceaneering, petrochemicals, oil and gas, and nuclear power engineering [2]–[6]. However, the practical application of this material at high temperatures is severely limited due to the poor thermal stability of unwanted precipitates, such as the σ phase and chromium nitrides, which can cause a significant reduction in toughness and corrosion resistance [7]–[10]. For the construction of various engineering structures, the weld joint of DSS is necessary. However, this process leads to complex thermal cycles that cause an imbalance of phase ratio and distortion of grain patterns in the DSS. Moon et al., [11] studied super duplex stainless steel welds made using tungsten inert gas (TIG). They found a correlation between the precipitation of the σ phase, pitting corrosion resistance, and microstructural change. The study showed that the favorable condition to form sigma phases is the post-weld heat treatment temperature at 930 °C. In a study conducted by Hosseini et al., [12] they examined the bead geometry and microstructure changes produced by thermal cycles in shielded metal arc welding of 13-mm super-duplex stainless steel (SDSS) using multiple passes. The results showed that reheating, whether through one or multiple passes, led to the development of a microstructure with both coarsened primary austenite and precipitated and/or coarsened secondary austenite. Additionally, they observed that the high-temperature HAZ in its as-welded state contained high fractions of ferrite with nitrides, but reheating caused nitride dissolution in HAZ with varying austenite fractions along the fusion boundary. Xie et al., [13] conducted a study on the microstructure and formation mechanism of DSS multi-pass weld joints. Their research revealed that there was a significant phase imbalance at the HAZ and weld fillers - the HAZ became fertilised while the weld fillers were dominated by austenite.

Nitrogen, which is one of the strongest austenite-forming alloying elements, is an economical and efficient substitute for nickel [14], [15]. It also contributes to high strength and corrosion resistance. If the weld metal contains an excessively high content of ferrite due to the loss of nitrogen during welding, it will negatively affect the mechanical and corrosion performance of DSS weldments. Pimenta et al., [16] reported an almost linear relationship between the increase in nitrogen content and the volume fraction of austenite in the weld metal. Topić & Knezović., [17] tested the ultimate tensile strength of 2205 duplex stainless steel produced with laser

welding and different combinations of shielding gases and suggested further research on the use of nitrogen in shielding gas. In their study, Brytan and Niagaj., [18] examined the corrosion characteristics of lean duplex stainless steel welded joints using potentiodynamic testing and electrochemical impedance spectroscopy. The results showed that the corrosion resistance of the TIG and Activated-TiG welded joints was lower when compared to the non-welded parent metal. However, by introducing the appropriate amount of heat input during welding and using shielding gases rich in nitrogen or helium, the austenitic phase content can be increased, which is beneficial for corrosion resistance and enhances surface oxide layer resistance. In a research study conducted by Gurrala et al., [19] tungsten inert gas (TIG) welding was performed using different shielding gas compositions to investigate the effect of the shielding environment on the protective qualities of passive films of 2205 DSS. The researchers found that the solubility of nitrogen in the weld increases with higher welding heat input and the addition of nitrogen to the shielding gas, which leads to an increase in austenite content. Additionally, they observed from electrochemical impedance spectroscopy (EIS) that the weld zone of Activated-TIG with $Ar+N_2$ shielding gas has much higher pitting corrosion resistance than TIG and Activated-TIG. Ravichandran et al., [20] studied the influence of TIG welding parameters on the mechanical properties of 2205 DSS using SN ratio and ANOVA analysis. Welding current, gas flow rate and welding speed were considered as the welding parameters and impact strength and hardness were taken as responses. From the SN ratio analysis, they concluded that the high impact strength can be obtained when the welding current was 150 A, the gas flow rate was 14 L/min, and the welding speed was 210 mm/min. However, they also found the high hardness of the weldmens could be obtained when the welding current was 190 A, the gas flow rate was 12 L/min, and the welding speed was 175 mm/min. In a study conducted by Mondal et al., [21], the optimal process conditions for Tungsten Inert Gas (TIG) welding of (DSS) were determined to achieve the desired mechanical properties of the weld. The researchers utilized the Grey-based Taguchi methodology for process optimization to solve the multi-response optimization problem. They carried out an ANOVA test to identify the significance of each factor on the desired responses. The study found that the welding parameters yielding the highest yield and ultimate tensile strength were welding current of 90A, gas flow rate of 8 L/min, and welding speed of 3.5 mm/s. Additionally, the study concluded that welding speed was the most significant factor influencing the optimization of the welding process.

In a previous study, the authors researched the impact of various TIG welding process parameters on the corrosion resistance of DSS weldments. They used the potentiodynamic polarization technique and concluded that the WC and N_2 are the most significant parameters

that affect the corrosion penetration rate. The study also found the optimal value of TIG welding parameters that reduce the CPR obtained using the potentiodynamic polarization technique. Therefore, the objective of this study is to optimize and analyze the effect of TIG welding process parameters on the corrosion resistance of duplex stainless steel weld joints using the electrochemical impedance technique through response surface methodology.

2. Material and experimental procedure:

2.1. Material and welding process:

The research conducted used duplex stainless steel DSS 2205 (UNS S32205) as the work material for the experiments. The chemical compositions of the base metal (BM) are shown in Table 1. The base metal was machined into plates of 6.35×140×50 mm using an Abrasive Water Jet cutting machine with a double-V butt weld joint. Before welding, the plates were cleaned mechanically to remove rust and other contaminants. A schematic diagram of the welding process shown in Fig 1.

Table. 1: Chemical composition of duplex stainless steel

Component	Cr	Ni	Mn	C	Si	P	Mo	Cu	N	Fe
Wt%	22.2	4.70	1.72	0.03	0.037	0.03	2.55	0.2	0.17	68

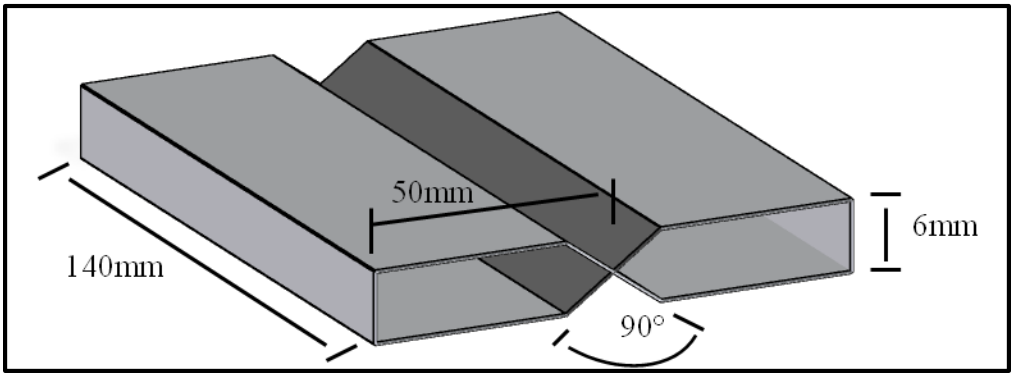

Figure. 1: Schematic diagram of the welding process

During the welding process, a TIG welding machine identified as DWHP250NL was used. A 2.4 mm tungsten electrode with an 8 mm cup size was utilized, and the constant arc gap was maintained at 2 mm. The filler material used in this study was ER2209, which was 1.6 mm in size. The composition of the ER2209 filler material is listed in Table. 2.

Table. 2: The chemical composition of filler material

Components	C	Mn	Si	Cr	Ni	Mo	N	P	S	Fe
(wt%)	0.02	1.6	0.5	23	8.5	3.1	0.11	0.01	0.005	Balance

2.2. Experimental design:

An approach called response surface method (RSM) was used to plan welding experiments for duplex stainless steel. The experimental design matrix was developed using RSM's central composite rotatable design (CCD). Three factors were varied at five levels, resulting in a CCD matrix that included 8 cube points, 6 center points in cube, and 6 axial points. The study focused on three input parameters: welding current WC, welding speed WS and the amount of N_2 added to Ar as shielding gas. The flow rate for the gas remains constant at 10 l/min. 20 butt-welded samples have been produced, using five different levels of the above mentioned parameters. The corrosion rate has been measured and serves as the response variable. The levels of factors were determined based on trial runs and literature review, as shown in Table. 3.

Table. 3: The range values of welding process parameters

NO	***Input Parameter***			***levels***		
		-2	-1	0	1	2
1	Welding current (A)	140	155	170	185	200
2	Welding speed (mm/min)	135	155	175	195	215
3	N_2 (%)	0	5	10	15	20

After entering the factorial levels for each input variable into MINITAB_19 software, we obtain the matrix of input experiments for welding processes. Table. 4 presents the matrix of welding process experiments.

Table. 4: The matrix of welding processes experiments

No	***Welding current (A)***	***Welding speed (mm/min)***	***N_2 %***
1	185	155	15
2	170	175	10
3	200	175	10
4	155	195	15
5	170	175	0
6	170	215	10

7	170	175	10
8	170	175	10
9	140	175	10
10	170	175	10
11	170	175	10
12	185	195	5
13	185	195	15
14	170	175	20
15	185	155	5
16	155	195	5
17	170	135	10
18	170	175	10
19	155	155	15
20	155	155	5

2.3. Microstructure examination:

The samples for microstructure observation were cut from the original DSS weldments using a water jet-cutting machine. To clarify and illustrate the results, the microstructure of the samples with high and low corrosion rates was imaged using an OLYMPUS BX61 optical microscope and an EP50 digital camera. The samples were ground and polished in accordance with the ASTM-E407-2002 standard using silicon carbide abrasive sheets with grit sizes ranging from 240 to 1200. Water was used as a lubricant and coolant. The samples were cleaned with water, then polished with diamond paste and cooling oil using 3mm and 1mm billiard cloth to achieve a smooth, mirror-like finish on the sample surfaces. Beraha's etching solution, consisting of 1g of $K_2S_2O_5$, 15 ml of HCl, and 85 ml of distilled water, was used to dip the samples.

2.4. Corrosion test:

Electrochemical Impedance Spectroscopy (EIS) is a widely recognized quantitative technique that helps in the quick evaluation of the anti-corrosion performance of protective coatings and alloys with a passive film, such as stainless steels. EIS measurements provide reliable data in

short testing times, which allows for accurate prediction of the long-term performance of the passive film. (EIS) was conducted in accordance with the guidelines of ASTM G106. The test was carried out for 5 hours at open circuit potential in a conventional three-electrode cell containing 3.5% NaCl. The welded specimens were used as a working electrode (WE), while a saturated silver/silver chloride electrode and a graphite rod were utilized as a reference and counter electrode respectively. The welded samples, including the weld zone and HAZ, were cut into approximate dimensions of 20 mm × 15 mm × 6 mm. A copper wire was attached to one end by spot welding to create an electrical connection. The wire was then covered with a plastic tube, and the samples were mounted using polystyrene molding epoxy to insulate all sides except the area exposed to the electrolyte. After that, the samples were mechanically ground using a range of SiC emery papers, from 320 to 800 grits, and polished with DP-Lubricant blue. They were then rinsed in distilled water, cleaned ultrasonically with alcohol, and dried in air. EIS measurements were taken at the open circuit potential, ranging from 100 kHz to 10 MHz, using a peak-to-peak voltage excitation of 10 mV. The semi-circuit Nyquist plot was fitted using ACM analysis software with the circuit fit bottom to obtain the equivalent circuit and corrosion rate.

3. Result and discussion:

The electrochemical impedance technique was used to determine the corrosion rate results. The corrosion penetration rate (CPR) refers to the amount of metal lost per year in thickness. The Electrochemical Impedance Spectrum (EIS) is a powerful technique that measures the resistance of metals and alloys against corrosion. The corrosion rate of DSS weldments is directly influenced by changes in welding parameters. Therefore, it is essential to develop a mathematical model that describes the relationship between welding parameters and the corrosion rate of DSS weldments. Table 5 presents the results of welding experiments and the corresponding corrosion rates.

Table. 5: Experiments and corrosion penetration rate results

No	***Welding Parameters***			***Response***
	welding current (A)	***welding speed (mm/min)***	***N_2 (%)***	***CPR_{EIS} mm/y***
1	185	155	15	0.00525
2	170	175	10	0.00480

3	200	175	10	0.00525
4	155	195	15	0.00480
5	170	175	0	0.00600
6	170	215	10	0.00330
7	170	175	10	0.00460
8	170	175	10	0.00385
9	140	175	10	0.00700
10	170	175	10	0.00365
11	170	175	10	0.00290
12	185	195	5	0.00320
13	185	195	15	0.00180
14	170	175	20	0.00550
15	185	155	5	0.00590
16	155	195	5	0.00550
17	170	135	10	0.00420
18	170	175	10	0.00450
19	155	155	15	0.00440
20	155	155	5	0.00500

3.1. Microstructure characterization:

Fig. 2 shows the microstructure of the design point 9 (from Table 3) that has high CPR and the design point 13 (from Table. 3) that has low CPR.

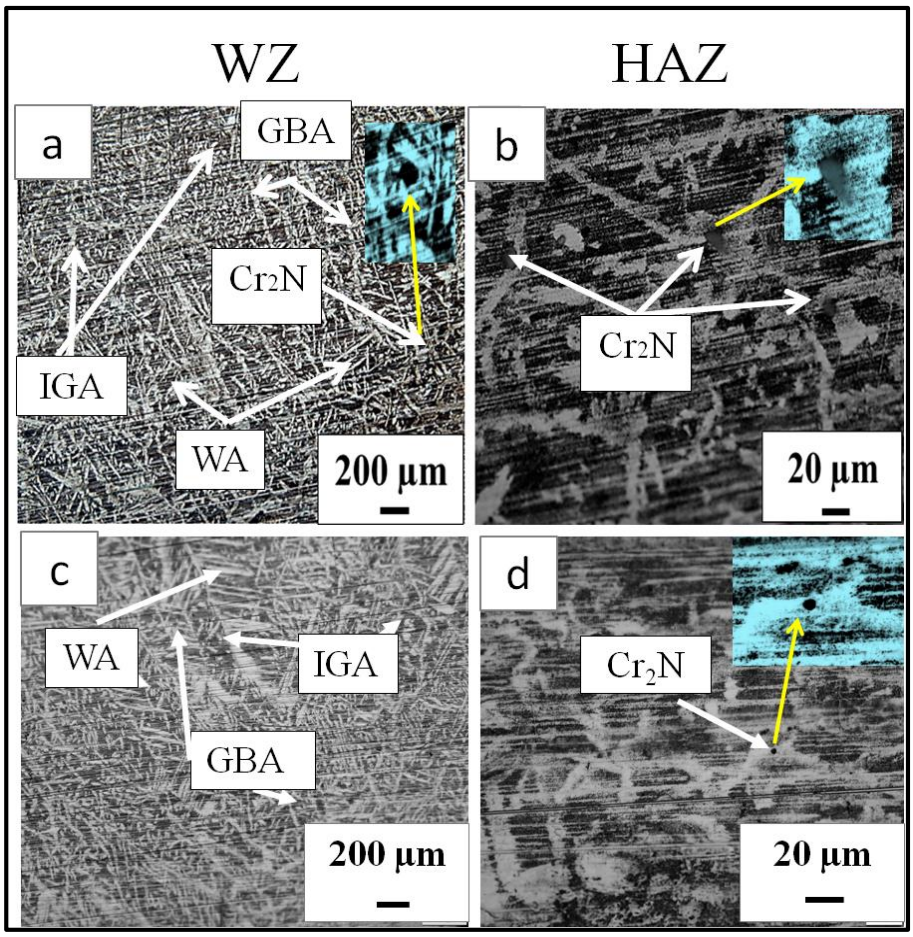

Figure. 2. Microstructure of the design points exhibit high and low CPR: (a) WZ of the design point 9, (b) HAZ of the design point 9, (c) WZ of the design point 13, (d) HAZ of the design point 13

Fig. 2(a) and 2(b) display the microstructures of WZ and HAZ of design point 9, which exhibit a high CPR. This design point has a large amount of Cr_2N precipitations in Weld and Heat-Affected Zones, as shown in Figure 2(a) and 2(b). Additionally, the austenite volume fraction of this design point is 51%. On the other hand, Figures 2(c) and 2(d) depict the microstructures of WZ and HAZ of design point 13, which have a low CPR. From the microstructure of WZ and HAZ shown in Figures 2(c) and 2(d), it can be clearly observed that a low amount of Cr_2N precipitations appear in HAZ. However, no Cr_2N precipitations have been observed in WZ. Furthermore, the austenite volume fraction of this design point is 57.4%. Therefore, the reduced CPR in DSS weldments is primarily due to the very high concentration of austenite and the absence of Cr_2N precipitations.

3.2 Analysis of variance ANOVA of the corrosion penetration rate:

The results of the analysis for a reduced quadratic model on the calculated corrosion rate values are presented in Table 6. As known statistically, P-value less than 0.05 generally indicate that model terms are significant, while P-value greater than 0.1000 indicate the terms are

insignificant. On the other hand, a high F-value for a parameter implies that the parameter has a high significant effect on the joint characteristics. The model analysis results show that the WC, WS, WC×WS, and $N_2 \times N_2$ are significant model terms. Table 6 also shows that the highest F-value is at a WC and WS of about 7.98, which means that they have the same effect, while N_2 is equal to 3.04, indicating statistically that the N_2 parameter has less influence on the CPR. Other model adequacy measures, such as R^2 and Adjusted R^2, are also presented in the Table 6. In general, the R^2 value indicates the model's goodness of fit. The value of R^2 for this model is 82.03%, which means that the model explains at least 82.03% of the variability in the response data. This shows that the proposed model is acceptable.

Table. 6: Analysis of variance for corrosion penetration rate

Source	***DF***	***Adj SS***	***Adj MS***	***F-Value***	***P-Value***
Model	6	0.000023	0.000004	9.89	0.000
WC (A)	1	0.000003	0.000003	7.98	0.014
WS (mm/min)	1	0.000003	0.000003	7.98	0.014
N_2 (%)	1	0.000001	0.000001	3.04	0.105
WC^2	1	0.000007	0.000007	17.17	0.001
$\mathbf{N_2^2}$	1	0.000004	0.000004	11.37	0.005
WC×WS	1	0.000006	0.000006	15.96	0.002
Error	13	0.000005	0.000000		
Lack of Fit	8	0.000002	0.000000	0.60	0.755
Pure Error	5	0.000003	0.000001		
Total	19	0.000028			
R^2=82.03%			R^2 (Adj)=73.74%		

3.3. Mathematical model of corrosion penetration rate:

A mathematical model has been developed to determine the corrosion penetration rate (CPR) of DSS weldments using linear, square, and interaction regression analysis. It is important to note that each parameter used in this mathematical model should fall within the range presented in Table 3. The equation for CPR has been expressed in terms of the welding process variables: welding current (WC), welding speed (WS), and nitrogen addition (N2).

$$CPR = -0.0078 - 0.000276WC + 0.000477WS - 0.000382N_2 + 0.0000002WC^2 + 0.000016N_2^2 - 0.000003(WC \times WS) \quad (1)$$

Where

(CPR) is corrosion penetration rate in (mm/y)

WC is welding current in (A)

WS is welding speed in (mm/min)

N_2 is nitrogen addition to argon in (%)

3.4. Three dimensional surface and contour plots:

A 3D surface plot is a valuable tool to predict the response value of any two parameters combined while keeping the third parameter constant. When the surface plot shows significant curvature, bend or undulations, it indicates a strong influence of these combined parameters. On the other hand, the contour plots are 2D plots where each contour line represents a constant response line. Fig. 3 (a) and (b) show the 3D surface and contour plots explaining the effect of the change in WC and WS at a constant middle value of N_2 on the behavior of CPR. Based on the 3D surface plot in Figure 3(a), it can be observed that the increase in WC combined with the decrease in WS, which corresponds to the high heat input, causes the CPR to increase due to the appearance of Cr_2N precipitations. Conversely, an increase in WS leads to a decrease in CPR due to relatively lower heat input, which reduces the appearance of Cr_2N precipitations. When WC is low, the decrease in WS leads to an increase in heat input, consequently resulting in a decrease in CPR due to the increase in austenite volume fraction and suppression of the appearance of Cr_2N precipitations. The contour plot shown in Figure 3(b) illustrates the same behavior as the surface plot of the CPR concerning the change in WC and WS at the constant N_2. Upon analyzing the plot, it is evident that increasing the value of WC more than 175A while also increasing WS above 190 mm/min results in a low value of CPR. Moreover, the same result can be obtained during the WC in the range of 145 to 160 A while decreasing the WS below 140 mm/min. Based on microstructure analysis, the increase in heat input increases the austenite content due to the slow cooling rate, but it can also contribute to the appearance of Cr_2N precipitation. The austenite phase of DSS weldments has a higher corrosion resistance compared to the ferrite phase. However, when the heat input is very low, the volume fraction of austenite reduces. To achieve a low value of CPR in DSS weldments, the appropriate heat input should be used to obtain a high content of austenite with a low amount of Cr_2N precipitation.

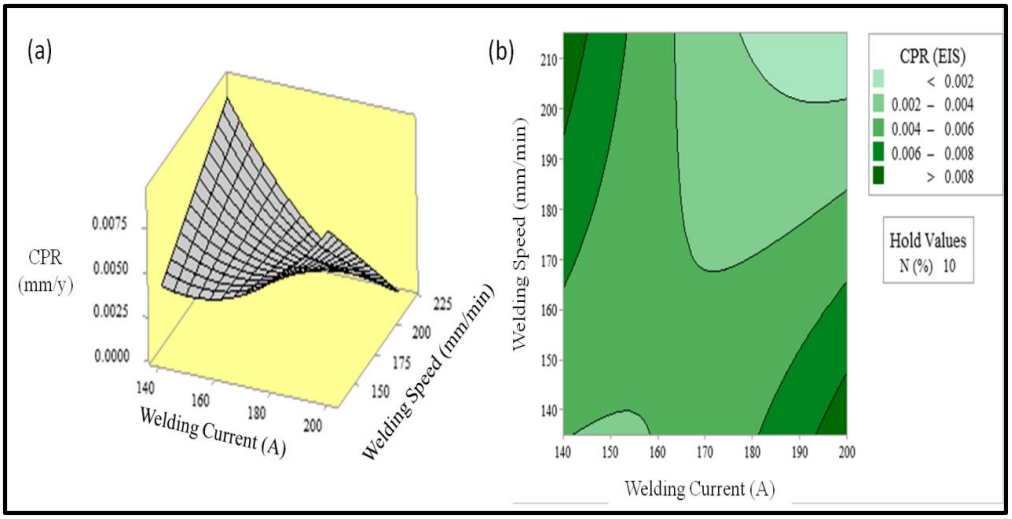

Figure. 3: CPR behavior versus WC and WS: (a) 3D surface plot, (b) 2D contour plot

Fig. 4(a) and 4(b) show 3D surface and contour plots that illustrate the effect of changing WC with N_2 at a constant WS on the behavior of CPR. The surface plot in Figure 4(a) shows that decreasing N_2 and WC leads to an increased CPR. This is due to an increase in the volume fraction of the ferrite phase, which has low corrosion resistance. Conversely, increasing WC with an increase in N_2 addition to Ar as a shielding gas also leads to an increase in CPR due to the increase in the appearance of Cr_2N precipitations. According to the surface plot, the lowest CPR can be achieved by using a middle value of WC and N_2. Adding N_2 with Ar as shielding gas can compensate for the loss of nitrogen from the weld pool, increase the driving force of the austenite phase, and subsequently decrease the CPR. However, the results of this study indicate that an increase N_2 leads to an increase in CPR, mainly due to the reappearance of the precipitation. Furthermore, the contour plot in Figure 4(b) indicates that to achieve the lowest CPR value, it is necessary to increase the value of WC to above 160 A but less than 190 A, and increase the amount of N_2 addition to above 5% but less than 15%.

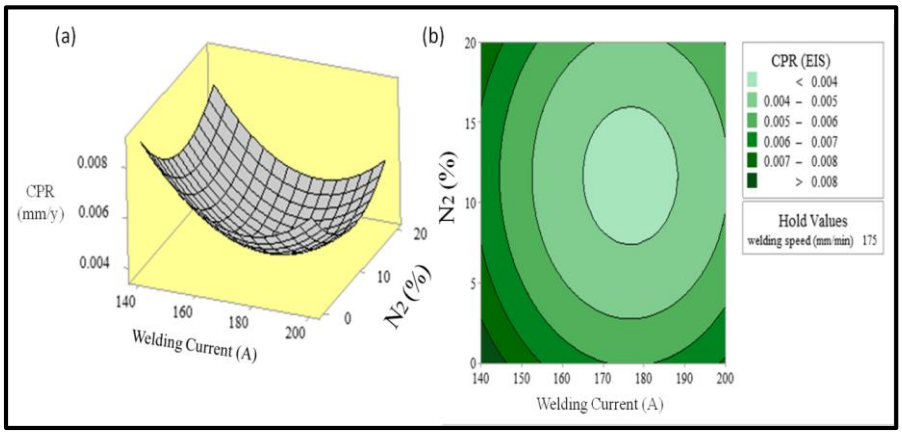

Figure. 4: CPR behavior versus WC and N_2: (a) 3D surface plot, (b) 2D contour plot

Fig. 5(a) and (b) display how the behavior of CPR changes with the variation of WS and N_2 addition at a constant WC, represented through surface and contour plots. The 3D surface plot shown in Figure 5(a) indicates that at a high value of WS, the CPR initially increases at 100% Ar and then decreases as the amount of N_2 increases until it reaches 10% N_2. However, more than 10% of N_2 addition showed an increasing trend in CPR, mainly due to the reappearance of Cr_2N precipitations. Furthermore, the contour plot in Figure 5(b) reveals that a high value of WS, more than 210 (mm/min) with a range between 8 and 13% of N_2 addition, decreases the CPR.

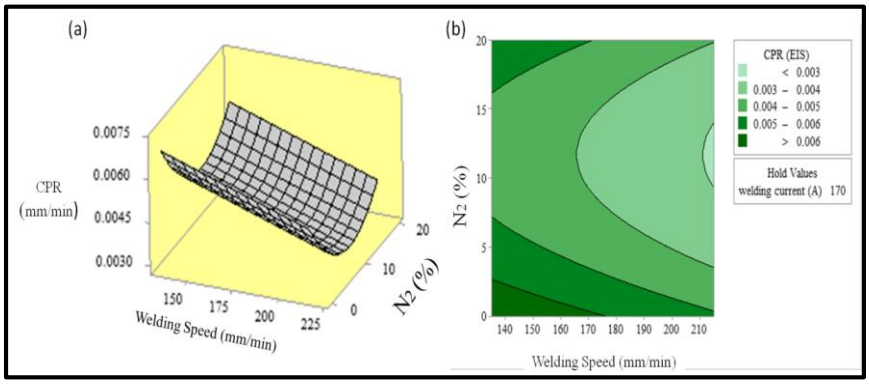

Figure. 5: CPR behavior versus WS and N_2: (a) 3D surface plot, (b) 2D contour plot

3.5. The corrosion penetration rate optimization:

Figure 6 displays the optimization plot, which shows the impact of each parameter on the response. The perpendicular red lines on the plot indicate the current parameter setup, and the red values at the top of each column represent the current parameter values. The blue dashed line and blue values indicate the responses for the current parameter values. A desirability (D=1.00) indicates that the welding parameters' combination is good, satisfying a CPR optimum and effectively minimizing CPR. From the optimization plot shown in Figure 6, it can be observed that the optimal values for WC, WS, and N_2 addition are 200A, 215mm/min, and 12%, respectively. These values resulted in the lowest CPR of 0.0005 mm/y. The model clearly shows that adding a small amount of N_2 with an appropriate welding process heat input results in high austenite content with a low amount of Cr_2N precipitation, which leads to a high corrosion resistance of DSS weldments.

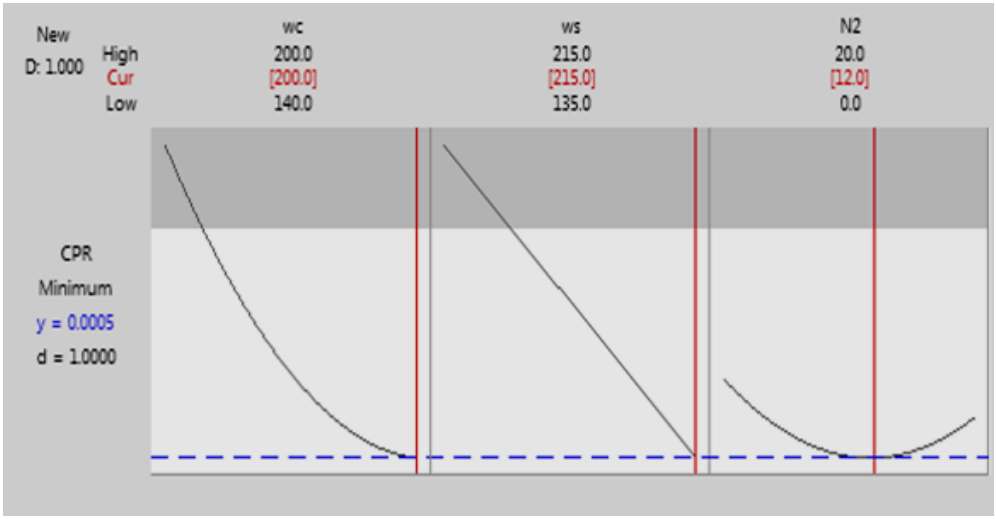

Figure. 6: The optimization plot of CPR Versus WC, WS, N_2

4. Conclusions:

A study was conducted to analyze the effect of TIG welding parameters on the corrosion resistance of duplex stainless steel DSS weld joints using Response Surface Methodology RSM. The corrosion resistance of DSS weldments was measured using the electrochemical impedance spectroscopy (EIS) technique, which explained through corrosion penetration rate. The main conclusions of the study:

1. The results showed that the electrochemical impedance technique is a powerful technique used to measure and predict the corrosion penetration rate of DSS weldments
2. The RSM results indicated that the welding parameters WC and WS are statistically more significant than N_2 addition on the corrosion penetration rate.
3. The accuracy of the model created using RSM is 82%, which means it is statistically acceptable.
4. Increasing WC while decreasing WS, which means high heat input, leads to a high CPR due to the Cr_2N precipitations' appearance. On the other hand, decreasing WC while increasing WS, which gives low heat input, also leads to a high value of corrosion penetration rate due to an increase in ferrite volume fraction.
5. The addition of a small amount of N_2 to argon as shielding gas showed benefits on the corrosion resistance of the DSS weld joint by decreasing the CPR. However, an increase in the amount of N_2 leads to an increase in the CPR due to the reappearance of the Cr_2N precipitations.

6. The RSM results indicated that the optimal welding parameters were WC=200A, WS=215 mm/min, and N2 of approximately 12%, which resulted in the lowest corrosion penetration rate of 0.0005 mm/y.

5. References:

(1) E. M. Westin, "Microstructure and properties of welds in the lean duplex stainless steel LDX 2101." KTH, 2010.

(2) A. García-Junceda, C. Díaz-Rivera, V. Gómez-Torralba, M. Rincón, M. Campos, and J. M. Torralba, "Analysis of the interface and mechanical properties of field-assisted sintered duplex stainless steels," Mater. Sci. Eng. A, vol. 740, pp. 410–419, 2019.

(3) X. Zhang et al., "Microstructure and mechanical properties of TOP-TIG-wire and arc additive manufactured super duplex stainless steel (ER2594)," Mater. Sci. Eng. A, vol. 762, p. 138097, 2019.

(4) T. Zhou et al., "Controlled cold rolling effect on microstructure and mechanical properties of Ce-modified SAF 2507 super duplex stainless steel," Mater. Sci. Eng. A, vol. 766, p. 138352, 2019.

(5) A. Ameri, Z. Quadir, M. Ashraf, and J. Escobedo-Diaz, "Effects of load partitioning and texture on the plastic anisotropy of duplex stainless steel alloys under quasi-static loading conditions," Mater. Sci. Eng. A, vol. 752, pp. 24–35, 2019.

(6) R. Badyka, G. Monnet, S. Saillet, C. Domain, and C. Pareige, "Quantification of hardening contribution of G-Phase precipitation and spinodal decomposition in aged duplex stainless steel: APT analysis and micro-hardness measurements," J. Nucl. Mater. vol. 514, pp. 266–275, 2019.

(7) J. Michalska and M. Sozańska, "Qualitative and quantitative analysis of σ and χ phases in 2205 duplex stainless steel," Mater. Charact., vol. 56, no. 4–5, pp. 355–362, 2006.

(8) H. Sieurin and R. Sandström, "Sigma phase precipitation in duplex stainless steel 2205," Mater. Sci. Eng. A, vol. 444, no. 1–2, pp. 271–276, 2007.

(9) G. Fargas, M. Anglada, and A. Mateo, "Effect of the annealing temperature on the mechanical properties, formability and corrosion resistance of hot-rolled duplex stainless steel," J. Mater. Process. Technol., vol. 209, no. 4, pp. 1770–1782, 2009.

(10) R. Badji, M. Bouabdallah, B. Bacroix, C. Kahloun, K. Bettahar, and N. Kherrouba, "Effect of solution treatment temperature on the precipitation kinetic of σ-phase in 2205 duplex stainless steel welds," Mater. Sci. Eng. A, vol. 496, no. 1–2, pp. 447–454, 2008.

(11) I. J. Moon, B. S. Jang, and J. H. Koh, "Heat treatment effect on pitting corrosion of super duplex stainless steel UNS s32750 GTA welds," in Advanced Materials Research, 2013, vol. 746, pp. 467–472. doi: 10.4028/www.scientific.net/AMR.746.467.

(12) V. A Hosseini, K. Hurtig, and L. Karlsson, "Bead by bead study of a multipass shielded metal arc-welded super-duplex stainless steel," Weld. World, vol. 64, no. 2, pp. 283–299, 2020.

(13) X. Xie et al., "Nonhomogeneous microstructure formation and its role on tensile and fatigue performance of duplex stainless steel 2205 multi-pass weld joints," Mater. Sci. Eng. A, vol. 786, p. 139426, 2020.

(14) H. Hänninen, J. Romu, R. Ilola, J. Tervo, and A. Laitinen, "Effects of processing and manufacturing of high nitrogen-containing stainless steels on their mechanical, corrosion and wear properties," J. Mater. Process. Technol., vol. 117, no. 3, pp. 424–430, 2001.

(15) J. Li, Z. Ma, X. Xiao, J. Zhao, and L. Jiang, "On the behavior of nitrogen in a low-Ni high-Mn super duplex stainless steel," Mater. Des. vol. 32, no. 4, pp. 2199–2205, 2011.

(16) A. R. Pimenta, M. G. Diniz, G. Perez, and I. G. Solórzano-Naranjo, "Nitrogen addition to the shielding gas for welding hyper-duplex stainless steel," Soldag. E Insp., vol. 25, pp. 1–8, 2020, doi: 10.1590/0104-9224/SI25.12.

(17) A. Topić and N. Knezović, "31ST DAAAM International Symposium On Intelligent Manufacturing and Automation Influence of Shielding Gas Mixture Type on Ultimate Tensile Sterngth of Laser-Welded Joints in Duplex Stainless Steel 2205," 2020, doi: 10.2507/31st.daaam.proceedings.xxx.

(18) Z. Brytan and J. Niagaj, "Corrosion studies using potentiodynamic and EIS electrochemical techniques of welded lean duplex stainless steel UNS S82441," Appl. Surf. Sci., vol. 388, pp. 160–168, 2016.

(19) A. K. Gurrala, A. Tirumalla, S. Sheik, and R. Mohammed, "Effect of shielding environment on microstructure and corrosion behaviour of 2205 duplex stainless-steel weldments".

(20) M. Ravichandran, A. Naveen Sait, and U. Vignesh, "Investigation on TIG welding parameters of 2205 duplex stainless steel," Int. J. Automot. Mech. Eng., vol. 14, no. 3, pp. 4518–4530, Sep. 2017, doi: 10.15282/ijame.14.3.2017.10.0357.

(21) S. Mondal, P. K. Pal, and G. Nandi, "Optimization of process parameters of TIG welding of duplex stainless steel without filler rod by grey-Taguchi method," Indian J. Eng. Mater. Sci., vol. 28, no. 4, pp. 385–392, 2021.

(22) M. S. Melad, M. A. Gebril, F. M. Shuaeib, F. I. Haidar, D. M. Elabar, and S. M. Elkoum, "Parametric Study and Optimization the Effect of TIG Welding Process Parameters on the Corrosion Resistance of 2205 DSS Weldment using Potentiodynamic Polarization Technique," Sci. J. Univ. Benghazi, vol. 36, no. 2, 2023.